We welcome constructive feedback: corresponding emails can be addressed to stephenjudsonturner@gmail.com

Volcanic arc structure controlled by liquid focusing from the slab — evidence from boron isotopes and trace elements

Stephen J. Turner[1,2], Ivan P. Savov[3], Tamsin A. Mather[4], Richard F. Katz[4], David W. Rees Jones[5], Davis M. Pyle[4], Jan C. M. de Hoog[6], Sebastian F. L. Watt[7]

Affiliations: [1]University of Houston, [2]University of Massachusetts Amherst, [3]University of Leeds, [4]University of Oxford, [5]University of St. Andrews, [6]University of Edinburgh, [7]University of Birmingham

A research report for submission to *Proceedings of the National Academy of Sciences*

Keywords: Subduction, Volcanism, Volatile Cycling

Abstract (250 words)

The rates and pathways of material transport from subducting plates to arc volcanoes control the long-term chemical evolution of the atmosphere, continents, and mantle. Arc magma compositions are commonly used as proxies for the state of the slab directly below a volcanic vent, under the assumption of vertical transport from the slab to the surface. Here, we present new boron (B) isotope and trace element data that challenge this assumption. Measurements of olivine-hosted melt inclusions from 900 km along and 200 km across the Southern Andean Volcanic Zone reveal remarkably coherent trends, indicating: (1) That the B isotope composition of the slab component sampled by erupted magma is invariant with slab depth, contrary to the expectation that the slab composition should progressively change with dehydration, and (2) that slab overprinting decreases with the distance from a long-lived arc-front stratovolcano in both along- and across-arc directions. These observations indicate that slab liquids generated across a large depth range are subsequently homogenized and focused both parallel and perpendicular to the trench. Similar geochemical behavior is apparent in other arc segments. We hypothesize that along-arc focusing is the consequence of periodic-in-space, solid-state, abortive upwelling from the slab surface, and that this produces persistent zones of elevated mantle melting consistent with the characteristic narrow geometry and isolated, long-lived stratovolcanoes of volcanic arcs. This framework implies that the structures of volcanic arcs have a deep origin, and can be used to better interpret global variations in subduction fluxes and their relationship with subduction parameters.

Significance Statement (120 words)

When Earth's tectonic plates sink (subduct) into the mantle, a series of mineral reactions produces liquids that trigger melting and 'arc' volcanism. Over time, material transfer between subducting plates and upwelling magma has shaped the Earth's structure and geochemistry, though many details are poorly understood. We measured volcanic rock samples from a large region spanning Chile and Argentina. We specifically utilized measurements of boron isotopes, which uniquely fingerprint materials impacted by subduction. Our results reveal new and unexpected details about the liquid pathways from the subducting plate and show that large arc volcanoes are fed by intensified magmatism that occurs when fluids from the subducting plate become focused from across a wide region as they ascend through the mantle.

Introduction

The evolution of our planet has been fundamentally shaped by the processes that partition subducting materials between volcanic arcs and the deep mantle. Advances in our understanding of these subduction fluxes have been enabled by a combined approach of geophysical modeling and geochemical measurements (1). For example, numerical models predict variable slab temperatures beneath different arc volcanoes (2) that appear to be related to individual volcano or arc-averaged lava compositions (3, 4). This approach is complicated, however, by the possibility that liquids generated within the slab (aqueous fluids, hydrous melts, or supercritical liquids (5) do not migrate vertically from their point of origin (where the slab dehydrates or melts), which means that the slab materials sampled by an arc volcano could have been extracted from the slab across a large range of pressures and temperatures (6–9). It is also possible that slab liquids are unevenly distributed in the mantle along the length of volcanic arcs. This view is supported by seismic attenuation studies (10, 11) indicating that the abundance of slab liquids can vary significantly along the strike of an arc and may be more abundant in the mantle beneath areas of elevated magmatic flux. The few available studies that have utilized three-dimensional numerical models have arrived at similar conclusions (12, 13).

Slab liquids may therefore migrate both along- and across-strike of an arc front. The liquid migration pathways are not yet well understood, however, and are likely influenced by buoyancy, compaction pressure gradients, reactive infiltration instabilities, and a variety of other factors that can give rise to system self-organization and melt channelization (14–16). A complete understanding of the relationship between the geophysical parameters of subduction and the geochemical fluxes from the slab will therefore require sophisticated three-dimensional models that account for the complexities of two-phase flow. Analogous modeling approaches have greatly improved our understanding of magma generation and migration in mid-ocean ridge systems, but remain in their infancy for the relatively complex dynamics of subduction zones (14–17). Fundamental to testing such models are geochemical studies of volcanic arcs focused on geospatial systematics and chemical proxies that are sensitive to the origin (temperature, pressure, and lithology) of slab-derived materials that are ultimately incorporated into arc magmas. To this end, we have conducted a study of along- and across-arc variability of trace element and boron (B) isotope compositions of volcanic rocks from the Southern Andean Volcanic Zone (SAVZ) of Chile and Argentina.

In this study we show that, despite the particularly large scale of the study region, B isotope ratios and abundances in the SAVZ appear to be controlled by mixing between the background mantle and a compositionally homogeneous component from the subducting slab. Previously published B data from across-arc transects of the Marianas, Central America, Northern Japan, and Kamchatka can also be largely explained by two-component mixing between the slab and ambient mantle. The particularly clean result achieved by this study likely owes to our use of only olivine-hosted melt inclusions in their natural state, which may alleviate complications due to secondary alteration as well as undesirable side effects that can arise from experimental homogenization (18). At face value, the homogenous $\delta^{11}B$ of the slab component appears to contradict the results of numerical slab dehydration models developed by prior workers (19–21) as well as new models developed for this study, which all indicate that the B isotope composition of slab liquids should vary systematically due to isotopic fractionation as the slab sinks and dehydrates. To reconcile these modeling results with both new and previously published arc B measurements, we suggest that liquids generated within the slab across a large depth range are homogenized prior to reaching the mantle sources of the volcanics.

A second unanticipated result is that the extent of slab overprinting in the SAVZ diminishes with distance between a volcanic vent and the sites of long-lived, polygenetic arc-front stratovolcano, even when minor vents occur along the arc front. This result is supported by variations in B isotope compositions in melt inclusions as well as trace element compositions of whole-rock samples from a regional database. Similar whole-rock trends can be observed in a regional database from Eastern Mexico. This spatial variability indicates that slab liquids are preferentially focused into the mantle beneath arc-front stratovolcanoes. It follows that arc-front stratovolcano locations are importantly controlled by liquid-focusing mechanisms that begin at the surface of the subducting slab.

A multi-stage process accounts well for the observed geochemical and geospatial systematics. The homogeneity of the slab component across the arc may arise if early, shallow slab liquids are carried downward toward the arc front in regions of low porosity and late, deep slab liquids are deflected back toward the arc front by compaction pressure gradients that arise due to porosity gradients (6, 7, 9, 22). Along-arc focusing can be understood as a multi-stage process that begins with solid-state upwelling of buoyant material that is periodic with along-arc distance on the slab surface. Liquids emerging from the slab are deflected by the domed permeability barrier associated with the solid upwellings. Melt extraction

from the incipient upwellings leaves behind a dense, garnet-rich residual assemblage, preventing the upwellings from becoming long-lived diapirs. We show that this regional model for B isotope systematics can explain the geochemical variations across different volcanic arcs. This hypothesis and our geochemical constraints provide a direction for the development of fluid-dynamical models of subduction zones.

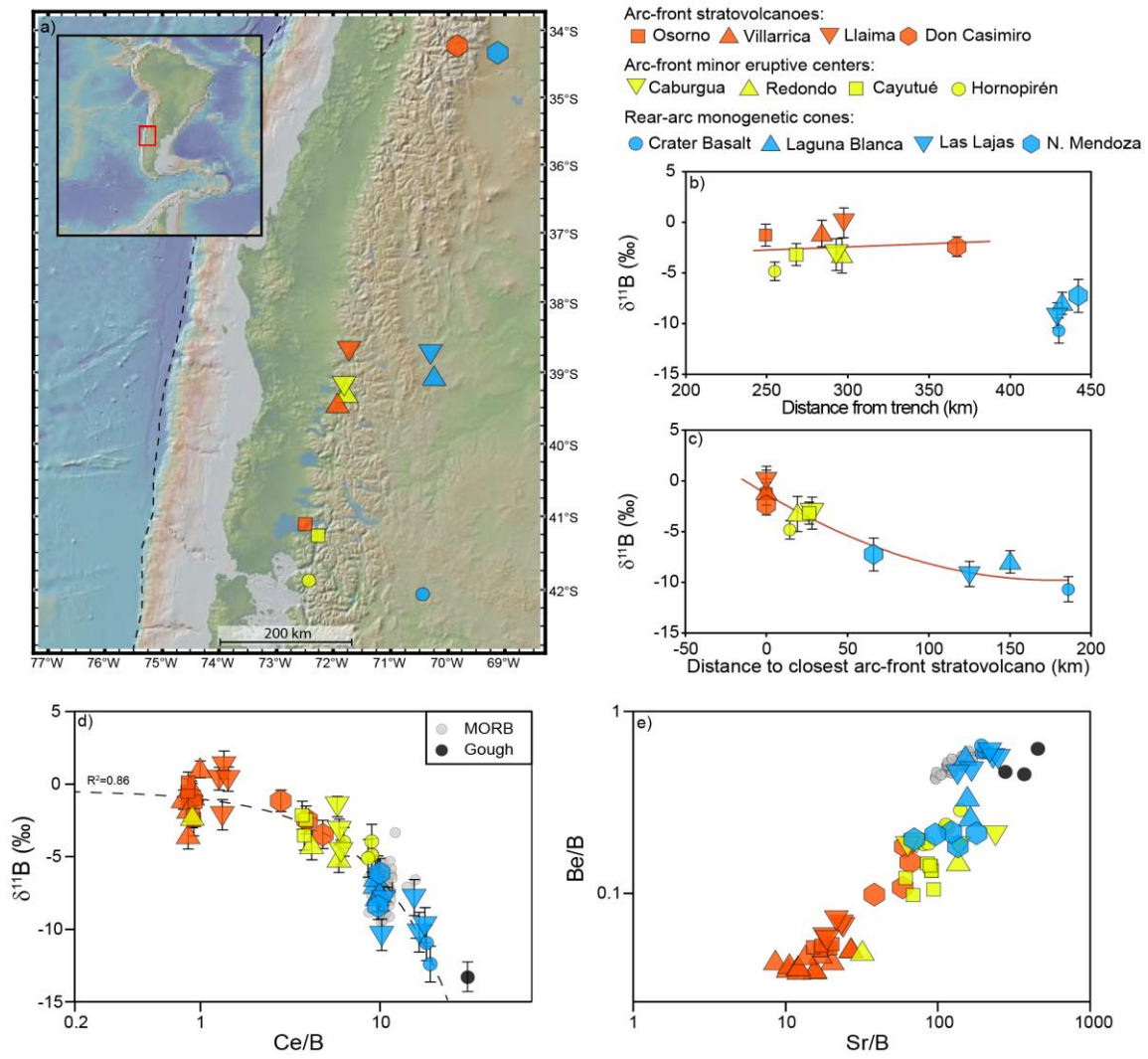

Figure 1. a) SAVZ regional map and sample sites. Dotted line denotes the location of the trench from (23). **b)** Sample-averaged $\delta^{11}B$ compositions vs. distance from the trench. Rear arc samples have consistently low $\delta^{11}B$, though no correlation is present among arc-front samples. Arc-front minor eruptive centers have consistently lower $\delta^{11}B$ than arc-front stratovolcanoes. Note that Hornopirén is adjacent to the much larger Yate volcano, which was not sampled for this study. **c)** Sample-average $\delta^{11}B$ decreases monotonically with distance from the nearest arc-front stratovolcano (red line is a second-order polynomial fit to the data). **d-e)** Linear geochemical trends (note log-linear scale in panel a, log-log in b) in $\delta^{11}B$ and B-normalized trace element abundances of SAVZ data. These trends support a model of two-component mixing between the ambient mantle that ranges from MORB to EM1-like (represented by Gough) and a homogeneous slab component with elevated $\delta^{11}B$.

1. The South Andean Volcanic Zone (SAVZ)

The South Andean Volcanic Zone (SAVZ, Fig. 1) is well-suited for regional studies focused on deep subduction processes. Its continental setting enables access to an array of smaller-volume volcanics both behind and along the arc front. Mafic volcanism that appears to be free of crustal contamination is present throughout the region (24–26). Volcanism has proceeded along the SAVZ in a relatively stable (27), accretionary (28) configuration for millions of years. The geochemistry of recent SAVZ volcanics are not affected by intra-arc rifting, as in the Cascades and Western Mexico (29), and only one volcanic center exhibits clear geochemical influences from subducting fracture zones (30, 31). The geochemistry of SAVZ volcanics should thus be a product of the larger-scale subduction geometry (26, 32–34), and the systematics of this arc should be relevant to other stable, long-lived subduction zones throughout Earth's history.

The SAVZ samples analyzed for this study can be categorized into three groups (Fig. 1): (1) scoria (and one lava, from Don Casimiro) that erupted from the edifices of major arc-front stratovolcanoes (2) scoria from minor eruptive centers on or near the arc front, and (3) scoria from rear-arc monogenetic cones. One analysis was also conducted on a sample from Gough Island, in the South Atlantic, because the ambient mantle (the mantle composition prior to mixing with slab components) of the SAVZ is heterogenous, with an enriched end member composition that resembles 'EM-1 type' Gough OIBs (24–26, 33, 35). All measurements were conducted on melt inclusions within olivine crystals. This approach mitigates the potential effects of crustal contamination and secondary alteration (36, 37).

2. Boron Isotopes

Boron was targeted for study because prior work has demonstrated that arc compositions are particularly sensitive to B contributions from the slab. Alteration of oceanic lithosphere produces hydrous minerals that have elevated B abundances, and subducting sediments also have ~100 times greater B abundances than typical upper mantle (38, 39). Boron is also one of very few elements expected to be mobile in both dehydration fluids and silicate melts under the full range of conditions in a subduction zone (40). Boron thus follows water into, within, and out of subducting slabs, and the large B budget of subducting plates can significantly overprint the composition of the mantle. The volume and source of slab-derived liquids that contribute to mantle melting and arc magma generation can thus be determined by analysis of arc magmas, which have notably higher B abundances than magmas from other tectonic settings (39). By analyzing samples from a large geographic region, it becomes possible to ascertain the large-scale processes that drive mantle melting and give rise to magmatic variability, elucidating the complex mechanisms at play during plate subduction and arc magma generation.

The B isotope system further aids the use of B as a subduction tracer. Boron's two stable isotopes (^{10}B and ^{11}B), are readily fractionated by lower temperature processes, including metamorphic dehydration reactions in subducting slabs (41). Boron isotope ratios are unlikely to be fractionated during mantle melting or early-stage crystal fractionation, however, so the B isotope ratios of unaltered basalts reflect the composition of their mantle sources. Mid-Ocean Ridge Basalt (MORB) measurements indicate a relatively uniform upper mantle composition with $\delta^{11}B$=-7.1±0.9‰ (relative to NIST SRM 951a), while Ocean Island Basalt (OIB) values are more variable, ranging from MORB-like values to $\delta^{11}B$≈-12‰ (38, 42, 43). Alteration of oceanic crust and/or lithospheric mantle shifts $\delta^{11}B$ values towards seawater, for which

158 $\delta^{11}B \approx 40‰$ (44). Altered oceanic crust thus enters the trench with elevated $\delta^{11}B$ (45, 46). Isotopic
159 fractionation during slab dehydration further concentrates ^{11}B into slab fluids (19). As a result, all $\delta^{11}B$
160 measurements of arc-front stratovolcano samples are higher than those of MORB and OIB, ranging up to
161 $\delta^{11}B = 17‰$ (39), clearly indicating B transport from the slab to the mantle source of arc magmas.

162

163 **3. Results**

164 Sample-averaged $\delta^{11}B$ values across the SAVZ range from -11‰ to +2‰. Rear-arc samples have
165 significantly lower $\delta^{11}B$ than samples from the arc front (Fig. 1b). There is not a strong SAVZ-wide
166 correlation between $\delta^{11}B$ and the distance to the trench (Fig. 1b). However, the average $\delta^{11}B$ of minor
167 eruptive centers are all lower than values from nearby arc-front stratovolcanoes, and there is an overall
168 trend among both arc-front minor eruptive centers and rear-arc cones of monotonically decreasing $\delta^{11}B$
169 with increasing distance from a long-lived polygenetic arc-front stratovolcano (Fig. 1c).

170 Boron abundances in arc volcanics can be normalized to elements with similar compatibility during mantle
171 melting such as Sr, Ce, Pr, and Be (24) to assess the relative influence of slab materials on the mantle
172 source. The B isotope and trace element ratios of the SAVZ melt inclusions form linear arrays on plots of
173 $\delta^{11}B$ vs Ce/B and Be/B vs Sr/B (Fig. 1d-e, note that the linear trend on Fig. 1d appears curved due to the
174 log-linear axis scales). The rear-arc SAVZ samples have the lowest $\delta^{11}B$ and plot between MORB (depleted
175 mantle) and EM-1 type (Gough Island) OIB compositions, as has also been found for other radiogenic
176 isotope and trace element ratios (24–26, 33, 35).

177

178 **4. Discussion**

179 Studies of arc lavas broadly agree that elevated B abundances and $\delta^{11}B$ in arcs reflect recycling of B from
180 the subducting plate, but there is no consensus yet regarding the causes of across-arc variations in $\delta^{11}B$
181 (18, 21, 37, 47–51). Lavas erupted from behind a volcanic arc front tend to have lower $\delta^{11}B$ than lavas
182 from the corresponding arc front, as seen in the SAVZ (Fig. 1b). These across-arc variations have been
183 interpreted by some as the result of changing slab fluid compositions from a progressively dehydrating
184 slab (20, 21, 37, 49, 50), while others have argued that across-arc variations reflect mixing between a
185 single slab component and the upper mantle (18, 47, 48, 51). The trends on Figure 1d-e are remarkably
186 well accounted for by mixing between two different chemical components, which always produces linear
187 arrays when both axes are normalized to the same element (see Figs. 1d-e). This data is not consistent
188 with more than two geochemical components unless additional end members are coincidentally co-linear.
189 Below, we demonstrate that geochemical models of slab dehydration do not produce multiple co-linear
190 components, and instead support the two-component mixing hypothesis.

191 Importantly, the linear across-arc trend in Ce/B vs. $\delta^{11}B$ (Fig. 1d) is not unique to the SAVZ, with similar
192 trends present (Fig. 2a) among samples from across-arc transects of El Salvador (52), Northern Japan (53),
193 and Northern Kamchatka (51). For these other arcs, the linear regressions through the arc data intersect
194 the compositional range seen in MORB, which suggests that the low-$\delta^{11}B$ end member in these arcs is
195 typical depleted upper mantle. While no rear-arc $\delta^{11}B$ data are available for the Marianas, variations in
196 Ce/B vs. $\delta^{11}B$ from the Marianas arc-front volcanics (54) also fall along a linear mixing trend

that intersects the MORB array (the Marianas are included on this plot due to the availability of fore-arc samples, discussed below).

Geochemical variability in $\delta^{11}B$ from other arcs can thus be accounted for by two-component mixing between a slab component and depleted mantle, just as in the SAVZ, though the $\delta^{11}B$ of the slab component appears to vary among arcs. In Fig. 2b, the y-axis is expanded to compare the data from Fig. 2a and the SAVZ to data from South Sandwich (55) and Nicaragua (18), for which all available samples are from arc-front stratovolcanoes with low Ce/B. The low Ce/B indicates that the B budget for these samples is dominated by the slab. Globally, the new SAVZ data reflect mixing to the lowest global (well-defined) slab $\delta^{11}B$ end member, with $\delta^{11}B \approx 0‰$, whereas South Sandwich reflects the highest global end member, with $\delta^{11}B \approx 15‰$. It is not yet known why some arc segments tend to have higher or lower $\delta^{11}B$ compositions (39). Below, we show that the regional interpretation of geochemical variability within individual arcs presented here provides a framework in which this global variability can also be better understood.

4.1. Across-Arc Geochemical Trends and Slab Liquid Pathways

The key observations relevant to across-arc transport of slab liquids in the SAVZ are 1) that rear-arc samples have much lower $\delta^{11}B$ than arc-front samples and 2) that covariations in $\delta^{11}B$ and B-normalized trace element abundances are linear. As highlighted above, this general interpretation of two-component mixing differs from some prior studies, which reasonably favored a systematically varying slab component across the arc. We suggest that the primary reason for these discrepant interpretations is that many older studies

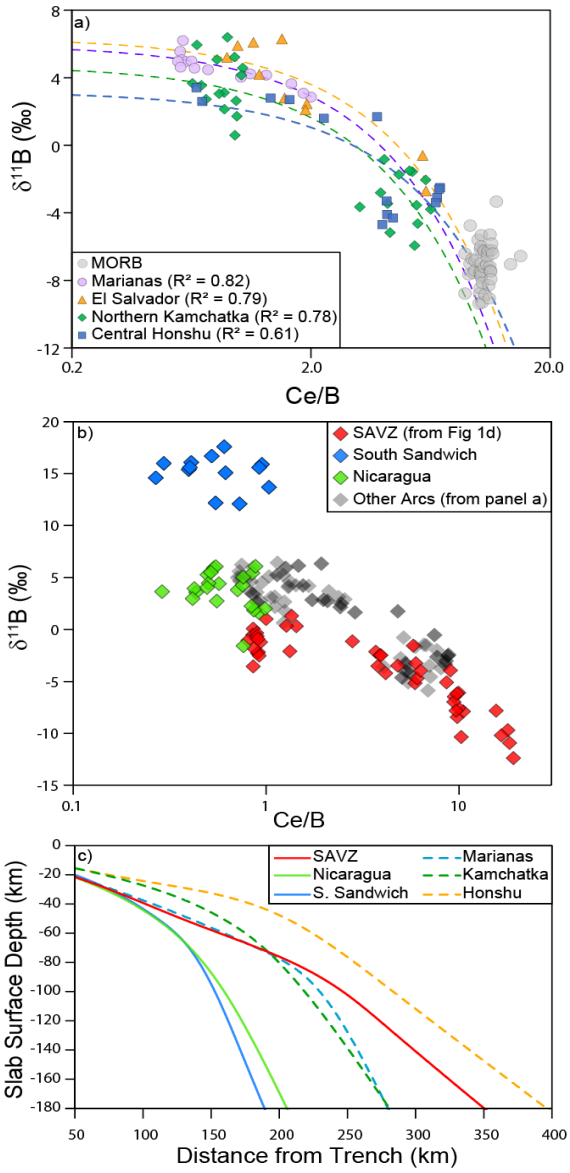

Figure 2. A comparison of B data and slab geometry among arcs. See text for data sources. a) $\delta^{11}B$ vs Ce/B in volcanic sample transects from other arcs. These arcs exhibit similar linear trends in $\delta^{11}B$ vs Ce/B. **b)** A comparison between SAVZ and the data from panel a. Also plotted are arc-front data from the South Sandwich Islands and Nicaragua, which have limited variance in Ce/B. Samples from South Sandwich have much higher $\delta^{11}B$ than measured in other arcs, while the Nicaraguan samples overlap with the data from panel a. **c)** A comparison of slab surface profiles. Slab geometry may have an important influence on slab dehydration and B isotope fractionation, though that Nicaragua and South Sandwich have significantly different $\delta^{11}B$ compositions despite similar steep slab profiles, while Honshu has a very shallow slab profile, but erupts samples that mix to a slab component with intermediate $\delta^{11}B$.

made use of the ratio Nb/B rather than Ce/B. The differences in the melt partitioning behavior between B and Nb (38) demonstrably produce large variations in Nb/B between enriched vs. depleted mantle sources (for a comparison of Nb/B and Ce/B data from this study, see Fig. S1, see also, (36)). The narrow range of Ce/B in MORB (38), on the other hand, indicates that this ratio provides a more reliable context for the interpretation of arc $\delta^{11}B$ data and supports a model in which regional $\delta^{11}B$ variability results from mixing between ambient mantle and a mostly homogenous slab component, as discussed above.

These two-component mixing arrays are a counter-intuitive result, because the continuous heating and dehydration of the slab should produce large swings in the $\delta^{11}B$ compositions of slab liquids (either fluids or melts) as subduction progresses. This occurs because ^{10}B is preferentially retained in the tetrahedral sites it occupies in its solid host minerals, as opposed to the trigonal configuration dominant in liquids (41). Liquids extracted from the slab at any depth will thus have higher $\delta^{11}B$ than the bulk dehydrating slab material. Progressive fluid loss from the upper layers of the slab will therefore cause the bulk slab composition and subsequent dehydration fluids or melts to continuously decrease in $\delta^{11}B$. Progressively lower $\delta^{11}B$ will also occur as increasing slab temperatures lead to less overall isotopic fractionation between solids and liquids (41). Finally, if the slab lithospheric mantle is serpentinized, as is commonly inferred (56, 57), the initial drop in $\delta^{11}B$ should be abruptly reversed at some point by the release of high-$\delta^{11}B$ liquid from deeper within the slab (21). Together, these processes will produce an initial drop in slab liquid $\delta^{11}B$ followed by a large upward spike, rather than a homogenous slab component that could serve as the end member of a linear mixing array.

Combined insights from thermo-mechanical models and experimental petrology can be used to quantitatively assess the progressive compositional evolution of slab liquids during subduction (18, 19, 21). Here, we demonstrate an example of this approach using the framework developed by (18) as applied to (58)'s thermo-mechanical model for the Marianas (selected given the unique constraints on the forearc fluid composition). The procedure involves building a dehydration model (Fig. 3a-b) based on the experimentally determined (or thermodynamically modeled) stability of hydrous minerals in the slab (59). These models show how the budget of structurally bound water in the slab decreases as the pressure and temperature increase. The rate of B loss and isotopic fractionation that occurs can then be calculated based on the slab temperature and the proportion of the mineral phengite (the main solid host of B) present at each interval of dehydration (19). The Ce/B ratio of slab liquids can be calculated from the modeled B and H_2O concentrations of slab liquids and the parameterization of liquid H_2O/Ce with pressure and temperature provided by (2). The model employed here has been improved slightly from that of (18) to account for re-equilibration of fluids as they traverse the slab, as in (21). Additional model details are available in the Materials and Methods Summary.

Figure 3c shows how slab liquid $\delta^{11}B$ evolves during progressive dehydration, assuming the liquids are extracted from the slab incrementally during subduction (symbol colors vary with the depth of liquid extraction). The calculated compositions follow the expected path of first decreasing (due to progressive heavy isotope depletion in the slab and higher temperatures), then increasing (due to the release of fluids from deep within the slab) $\delta^{11}B$. The $\delta^{11}B$ variations produced by this model agree well with previous modeling of the Kamchatka arc (21), despite differing subduction parameters and substantially different underlying assumptions in both the thermo-mechanical and geochemical models employed, which suggests that this general result is quite robust.

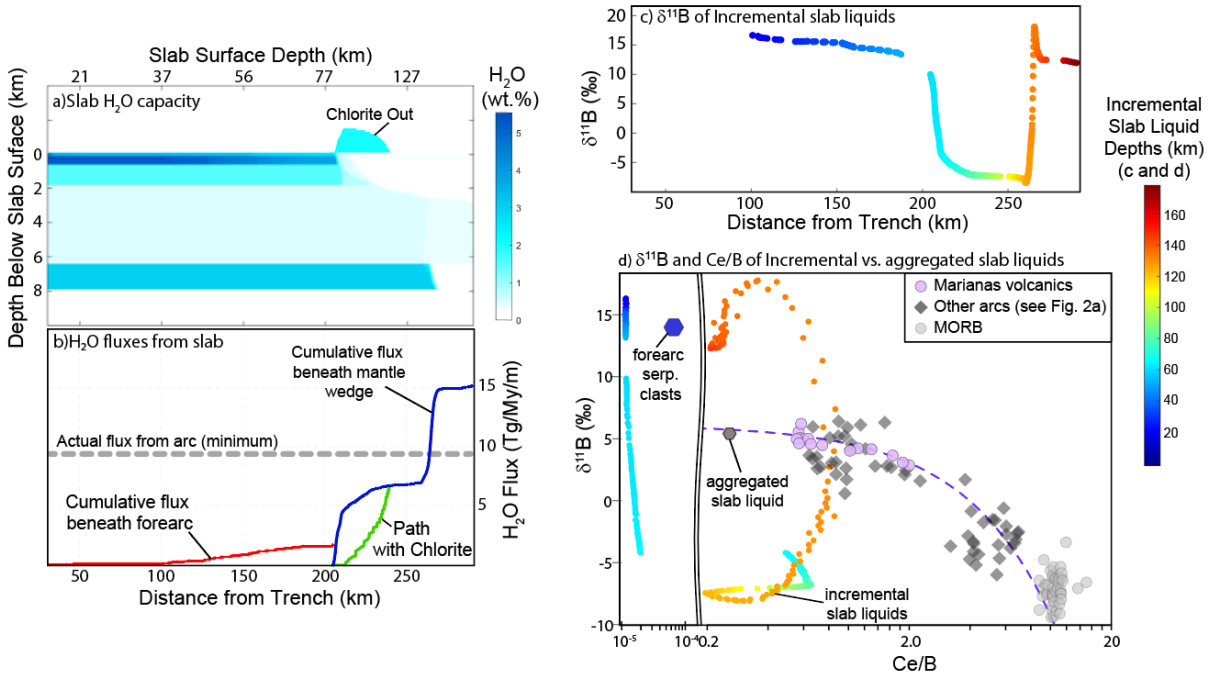

Figure 3. A comparison of global data and model results for different arcs. a) Linear trends are present in a) A slab dehydration model based on the geometry of the Mariana arc. The y axis refers to a position in or above the slab perpendicular to the slab surface, following (58), which is the source of the underlying thermal model. The model also shows the development and later dehydration of a chlorite-rich layer on the top of the slab. **b)** The H_2O flux delivered to the arc, assuming all water lost from the slab (starting from the coupling depth at 80 km depth and ~200 km from the trench) is delivered to the arc (based on the convergence rate for the Marianas). The model indicates two intervals of rapid fluid loss: one that occurs during the stage of rapid heating shortly after the coupling depth, and another for dehydration of the slab mantle lithosphere. Neither interval is predicted near the arc front, however, which lies 120-140 km above the slab (2). Even more importantly, water lost from both pulses must somehow be transported to the arc in order to account for the minimum flux of ~10 Tg/km/My that can be estimated from arc magma water contents and magma productivity. The gray line shows an estimate of the actual H_2O flux for the Marianas assuming primary magmas with 4.87 wt. % H_2O (3) and a magma production rate of 65 km^3/km/My. This magma production rate assumes a very minor (10 km^3/km/My) erosive/delamination losses over the lifetime of the arc, so 'true' values of magma production rate are likely higher(60). **c)** Model results showing the evolution of $\delta^{11}B$ in incremental slab liquids vs. distance from the trench. Points are color coded based on the slab surface depth per increment of dehydration. **d)** $\delta^{11}B$ vs Ce/B of model results and data. Note break in scale on the x axis. Small blue to red circles (see color bar legend to the right, and corresponding data in panel c) show the modeled compositions of 'incremental fluids' extracted at varying depths from the slab.

On Figure 3d, the incremental slab liquid $\delta^{11}B$ compositions are plotted vs Ce/B, which enables a direct comparison to the arc data. The model confirms that the linear arc data arrays on Figs. 2d and 3a are inconsistent with mixing between the mantle and "incremental" slab liquids, because the model compositions undergo swings of ~20‰ $\delta^{11}B$ in the proximity of both the arc front and rear arc, but remain consistently low in Ce/B. These incremental slab liquid compositions do not lie along a co-linear path with the arc data. Instead, the incremental liquids plot as an array that is orthogonal to the arc data. As such, mixing between the ambient mantle and these highly varied incremental slab liquids would produce scattered points on these plots rather than the linear correlations that are observed.

While the arc volcano data conflicts with the model of progressive variations in incremental slab liquid compositions (Fig. 3d), it is notable that the high $\delta^{11}B$ found in fore-arc serpentinites are well accounted for by shallow slab fluids. The Marianas serve as a useful example of this because the modern forearc

mantle is directly sampled as serpentinite clasts from mud volcanoes (61–63). These samples indicate a forearc with $\delta^{11}B$~+14‰ and extremely low Ce/B, in agreement with the modeled slab fluids lost at depths <60 km (Fig. 3c-d). Importantly, the Marianas forearc data do not lie along the linear trend produced by the arc front samples, and thus require a slab component that differs in composition from the deeper, homogenized end member delivered to the arc volcanics.

These contrasting forearc and arc-front compositions may indicate limited mass transfer between the forearc and mantle wedge. This would be consistent with across-arc heat flux data, which indicate a rapid shift in the geothermal gradient in between each arc front and trench (64). This rapid shift is best explained if the subducting plate initially slips beneath the overlying fore arc without coupling to it, and later becomes viscously coupled to the overriding mantle, driving wedge corner flow (65). The fore-arc material could thus remain stagnant and isolated from the deeper convecting mantle wedge, continuously receiving a small (66) influx of high-$\delta^{11}B$ dehydration fluids that differ from the slab component delivered to the arc.

The differing forearc composition indicates that slab liquids do change substantially with depth, however, so why is it that the slab components delivered across the volcanic arc are comparatively homogeneous? A definitive answer to this question is not yet available, though this observation is at odds with any model in which slab fluids or melts are transported vertically from the point at which they are generated within the slab.

Slab dehydration models (e.g., (59); Fig. 3a-b) and basic H_2O mass balance generally require some mechanism by which water-bearing slab liquids become focused from the broad across-arc region where they are generated into the narrow region of high magmatic flux that defines the arc front. This requirement arises because all available models produce intervals of slab dehydration that do not typically align with the locations of narrow arc-fronts (67), and because the amount of H_2O lost from each interval is far smaller than the magmatic H_2O flux from the arc. An example of this is illustrated in Fig. 3b, which compares the cumulative H_2O flux that is released from the slab as it subducts beneath the mantle wedge (blue line, Fig. 3b) to the minimum actual H_2O flux from magmatism along the volcanic arc. An initial interval of rapid slab dehydration occurs just after the slab-mantle coupling depth, where the slab rapidly increases in temperature. This initial interval occurs tens of km closer to the trench than any observed arc volcanism. Thus, if the model is accurate, there must be some mechanism that prevents these early fluids from ascending vertically and fluxing the overlying mantle.

Some of the early-released slab volatile budget can be transported to greater depths in the form of down-dragged chlorite forming in mantle hydration reactions immediately above the slab surface (68). The thermal model shows that chloritization cannot serve as a general mechanism to explain the location of the arc front, however, because the region of chlorite stability reaches its maximum water capacity shortly after the coupling depth, then shrinks gradually over a more prolonged interval as chlorite breaks down (Fig. 3b). Chlorite thus has the potential to smooth out the rate of early fluid loss from the base of the mantle wedge (compare, for example, the blue and green paths in Fig. 3d), but cannot serve as a general mechanism to transport water beneath the arc front, nor account for narrow arc widths.

Recent thermo-mechanical modeling studies have highlighted several mechanisms that may better explain across-arc liquid migration. Across-arc transport of slab materials can involve both down-dragging of early dehydration fluids and up-dip flow of liquids from the deeper slab behind the arc front. Two-dimensional models that track both solid and liquid flow show that the mantle above the subducting plate

may initially have low permeability due to small grain sizes and low fluid fractions, causing early dehydration fluids or slab melts to be dragged downward beneath the arc (6, 7, 22, 69). Deep slab liquids lost well behind the arc front can also be transported up-dip towards the arc via high porosity channels that form within the slab or sub-parallel to the slab in the overlying mantle (7–9, 22).

If slab liquids are instead transported toward the arc front from a large range of depths, then the volcanic H_2O flux can be balanced, and the homogenous $\delta^{11}B$ of the slab component can be accounted for. Across-arc focusing of slab liquids initially generated over a large range of slab depths would homogenize the composition of the slab component delivered to the arc by aggregating these fluids into a narrow region along the arc front, and would help to explain why arcs have similar structures despite differing predictions for the depths of slab dehydration reactions. To further test this hypothesis, the aggregated $\delta^{11}B$ and Ce/B composition of the slab liquids generated by the model in Fig. 3 was calculated by mixing the incremental slab liquids together (accounting for their individual masses). The aggregated slab liquid is equivalent to the composition of the cumulative slab liquid (blue line, Fig 3b) at the maximum distance from the trench, which easily accounts for the full flux of H_2O delivered to the arc front (Fig. 2b). Remarkably, the $\delta^{11}B$ and Ce/B composition of the aggregated liquid plots directly along the linear trend of the volcanic arc data (Fig. 3d). Mixing between the ambient mantle and the model's aggregated slab liquid thus accounts well for the arc data.

This model agrees with prior work that shows how the $\delta^{11}B$ of liquids generated within subducting slabs should change significantly (here, by >20‰) as subduction progresses. When $\delta^{11}B$ and Ce/B compositions of the liquids are considered in tandem, these compositional changes are clearly inconsistent with the geochemical variability exhibited by arc volcanics. The arc volcanics are best explained if liquids from a large range of depths instead become focused toward the arc front and mixed together into an aggregated slab component that then overprints the ambient mantle to varying degrees.

This result also confirms that the budget of B delivered to arc volcanics originates from different layers of the slab than most other elements. Variations in other elemental abundances and isotopic compositions such as Pb, Ba, and Th often cannot be accounted for without multiple slab components (e.g., (70–72)), whereas the linear mixing on B-normalized plots can be explained with a single slab component. The slab-to-arc fluxes of most other elements are substantially controlled by differing proportions or compositions of subducting sediments (73), however, whereas sedimentary B is largely lost during early dehydration to the forearc (18). Where regionally variable slab components are observed among arc lavas, they are generally confined to sediment-dominated elements and can usually be linked to regional variations in the subducting sediment composition or other features on the surface of the subducting plate, such as seamounts (73–75). These features can apparently impact the composition of the slab component even when aggregated across a large area. The dehydration model shows that the B budget of the slab component is instead largely derived from deeper slab layers within the igneous ocean crust (e.g., (76)). As such, the surficial slab features that give rise to sustained changes in the net compositional flux to the arc do not substantially impact the aggregated $\delta^{11}B$ composition of slab liquids.

4.2. Along-Arc Geochemical Trends and Slab Liquid Pathways

Across-arc focusing may explain how slab liquids with progressively changing compositions can become homogenized and delivered to arc front volcanoes, but it does not explain the regionally variable along-

arc distribution of the slab component. The minor eruptive centers along the SAVZ arc front have consistently lower $\delta^{11}B$ than neighboring arc-front stratovolcanoes (Fig. 1b-c) and plot along a linear trend on Figs. 1d-c. This suggests that the mantle sources of different volcanic centers along the arc front have been overprinted by different amounts of material from the slab. The finding that SAVZ arc-front minor eruptive centers generally sample mantle sources with smaller slab contributions corroborates findings from trace element and radiogenic isotope studies (24, 77–79). The evidence thus supports a heterogeneous distribution of slab liquids along strike of the arc, with 'wetter' mantle beneath areas that have more voluminous volcanism. The systematic geochemical and regional variations in lava geochemistry thus require that slab liquids become focused not only across the arc, but also along the strike of the arc front. Large-scale, three-dimensional channelization of slab liquids towards stratovolcanoes has also been proposed beneath Japan based on seismic attenuation data (10). It is thus possible that along-arc focusing of slab liquids is a common feature of subduction zones.

To test this hypothesis, we compiled whole-rock ICP-MS data from arc-front SAVZ stratovolcanoes and monogenetic cones. The ratio Th/Nb is used as an additional proxy for the magnitude of slab liquid overprinting of the mantle sources for each sample locality because Th and Nb have similar solid-melt partition coefficients (80) during mantle melting (unlike Nb and B). As a result, there is a limited range in the Th/Nb compositions of MORBs and OIBs (81). By contrast, nearly all arc-front stratovolcano lavas have high Th/Nb due to the transfer of slab melts to their mantle sources (82–84). This ratio is thus relatively unaffected by ambient mantle variability and peridotite melting processes while being highly sensitive to slab overprinting.

Figures 4a-b show that the whole-rock Th/Nb compositions of SAVZ minor eruptive centers also broadly decrease with distance from the nearest stratovolcano, even along the arc front. There is significant scatter in Th/Nb, which can be partially attributed to intra-lab biases and varying data quality. The Th/Nb dataset benefits from much greater sample density than $\delta^{11}B$ data, however, and clearly shows that SAVZ minor erupted centers laying the farthest from major arc-front stratovolcanoes have the lowest average Th/Nb. This supports the hypothesis that the mantle sources of these minor eruptive centers have generally received a smaller influx of slab liquids. It should be noted, however, that both stratovolcanoes and arc-front minor eruptive centers have consistently higher $\delta^{11}B$ and Th/Nb than typical MORB and OIB (which generally have Th/Nb<0.14), indicating some degree of slab overprinting along the entire length of the arc front.

To assess the applicability of this finding to other arcs, we have also compiled whole-rock data from the volcanics of Eastern Mexico, where small-volume volcanic centers are abundant and high-quality data are widely available (85). As seen in Figs. 4c-d, the same general trend of decreasing Th/Nb with distance from a stratovolcano is present. An interesting departure from this trend occurs within the Valle de Bravo-Zitacuaro volcanic field, however, where samples maintain high Th/Nb values for up to 50 km West of Xinantecatl (Toluca) Volcano before finally dropping off. Nevertheless, the multi-proxy finding of diminishing slab contributions away from stratovolcanoes seen for the SAVZ appears to also be supported by the Th/Nb systematics in Eastern Mexico.

Why might a compositionally homogeneous slab component be heterogeneously distributed along the arc front? It has been suggested that coalescence of fluid networks across a broad region (10, 11) due to reaction infiltration instability (16, 86–89) might explain the 'wet fingers' observed in the mantle wedge beneath Japan. However, while the factors controlling reactive channelization are complex, numerical and

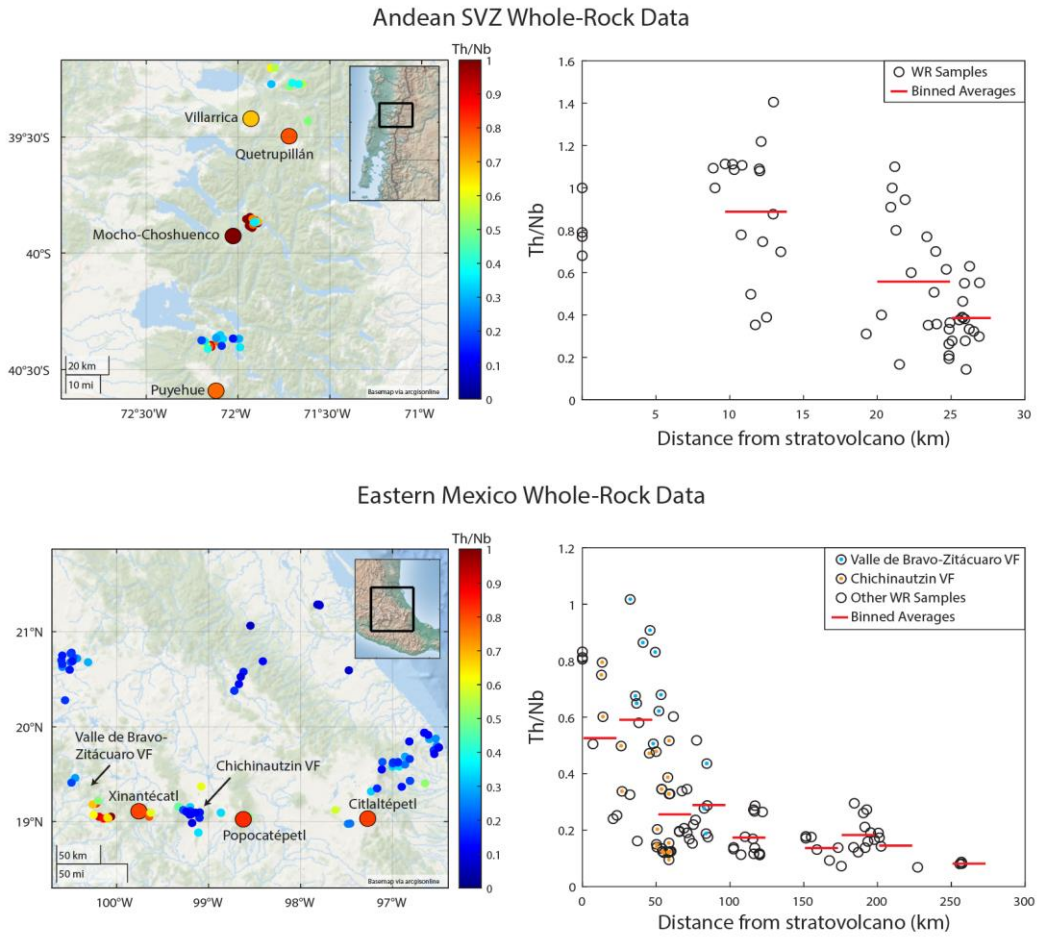

Figure 4. Whole rock Th/Nb data from **a)** the SAVZ and **b)** Eastern Mexico. Th/Nb is a proxy for the extent to which volcanic mantle sources have been overprinted by slab melts. Th/Nb values decrease with distance from the closest arc-front stratovolcano, just as seen for $\delta^{11}B$ (Fig/ 1). Only data with >3% MgO were included to mitigate the potential effects of crustal contamination. See text for discussion.

417

418 analytical treatments currently indicate that such melt networks might be limited to length scales that are
419 far smaller than the typical arc-front stratovolcano spacing (16, 90).

420 Another family of models invokes periodic upwelling of buoyant, low viscosity materials that subduct
421 along the surface of the slab. These can include sediments, altered oceanic crust, serpentinized peridotite,
422 or peridotite with trapped melt. A low viscosity, buoyant medium in such a layered arrangement has been
423 shown to upwell in periodic, domed protrusions with a wavelength that is a function of the relative
424 viscosities of materials and the underlying layer thickness (91, 92), and has long been proposed as a
425 possible mechanism to account for the spacing of arc volcanoes (93). From the original equations of Selig
426 (1965) (91), it can be shown that a spacing of 40 to 55 km, similar to the volcano spacing in the SAVZ,
427 would require a buoyant layer that is 3-4 km thick (given a relative viscosity contrast of 100, as in (94)).
428 More sophisticated three-dimensional numerical methods and experiments directly relevant to
429 subduction-zone geometries also support this general result, and show how in three dimensions these
430 upwelling protrusions can manifest as long-lived 'ridge-like structures' extending upward from the slab,
431 aligned perpendicular to the trench (12, 13, 95).

Instability calculations and tank experiments have been used to show that buoyant upwellings can theoretically develop into diapiric conduits (94, 96, 97), though this suggestion is not fully consistent with models that account for multi-phase flow and arc geochemistry. For example, the 3D models of Zhu et al. (12, 13) only predict full diapir formation when the mantle directly overlying the slab is assumed to fully retain a trapped melt, which conflicts with two-phase flow model implementations (7, 22). These two-phase flow models support an initial stage of melt retention above the slab, but find that the overlying mantle will eventually become permeable to rising liquids as the plate continues to subduct. Furthermore, all arc-front stratovolcano lavas have a sediment signature that is most consistent with a slab-derived sediment melt (98, 99), but the elemental fractionations observed between bulk subducting materials and melts are currently only produced experimentally at temperatures and pressures relevant to water-saturated melting at or near the surface of the slab (84, 100, 101). In addition, there is a growing body of evidence that suggests that melting commonly begins well beneath the slab surface, including melting of mafic ocean crust (84, 101–104). Quantitative modeling of arc compositions based on this assumption accounts well for the trace element and radiogenic isotope compositions of arc magmas (73, 75, 83).

Dehydration models such as Fig. 3b are also most consistent with fluid-saturated melting near the slab surface, because a large flux of water from the deeper slab layers is predicted across the same depth interval in which the slab surface exceeds the fluid-saturated solidus (84). Early slab melting such as this can be expected to arrest the ascent of buoyant diapirs because the melting reaction consumes buoyant phengite and quartz/coesite while producing dense garnet (105, 106). We propose that the most likely scenario, given the currently available models, experimental results, and geochemical observations involves a brief period of solid upwelling from the slab that coincides with an interval of water-saturated slab melting; upwelling then ceases after sufficient melt extraction.

Figure 5 depicts a conceptual model that can account for all the considerations above. This model is described in terms of three stages. In stage one (Fig. 5b), a buoyant layer 3-4 km thick is present that includes altered ocean crust, sediment, and a layer of chloritized peridotite. This buoyant layer begins to upwell periodically (93) with a wavelength that is comparable to arc stratovolcano spacing. In three dimensions, these upwellings manifest as long-lived ridges along the slab surface running perpendicular to the arc front (12, 13). This stage mirrors the initial phase of the diapiric models discussed previously. Shortly after reaching the slab–mantle coupling depth, the slab surface rapidly heats, causing the overlying chlorite to break down and the underlying sediment to begin melting. Upwelling of the thick buoyant layer will continue during the initial stages of slab melting, however, because the melt will be retained by an overlying mantle with low permeability.

In stage two (Fig. 5c), the permeability of the overlying mantle increases due to increasing fluid fractions and grain sizes (22). At this point, melts begin to ascend from the buoyant layer, despite the continued presence of a sharp permeability/porosity gradient. This configuration naturally gives rise to a sloped permeability barrier along the reaction front. Sparks and Parmentier (1991) and Spiegelman (1993) (107, 108) showed that a sloped, sublithospheric decompacting channel beneath a relatively impermeable lid can drive focused flow up the channel. In the context of mid-ocean ridges, two-dimensional numerical models have shown that this process can control melt focusing towards the ridge axis (109–111). In our proposed configuration, lateral focusing would lead to convergence of melt towards the center of the buoyant upwellings, driving along-strike variation in the flux of slab melts into the overlying mantle.

In stage three (Fig. 5d), continued melt extraction and the production of a dense garnet residue eliminates the buoyancy of the upwelling layer, arresting further ascent and preventing full diapir formation. This reconciles the theoretical considerations that support slab diapirs with the geochemical evidence favoring water-saturated melting near the slab surface detailed above.

In this conceptual framework, there is a smaller flux of slab melt to the regions between upwellings, consistent with the data from arc-front minor eruptive centers. Where the slab flux is low along the arc front, melts may remain trapped and transported by solid-state flow toward the rear-arc (6), which could explain why the slab component changes little in composition across the arc. A more rigorous geodynamical treatment of this problem will likely become possible over the next decade, as three-dimensional subduction zone models begin to integrate geochemical data and implement two-phase flow, including the effects of variable grain size, matrix compaction, melting, and melt–rock reaction.

4.3. Global Implications for B recycling in arcs

The context of across- and along-arc $\delta^{11}B$ systematics considered above motivates a re-evaluation of global $\delta^{11}B$ variability among arcs. While there is great diversity in B isotope compositions of samples from different arcs, most subduction zones around the world exhibit broadly similar two-component mixing systematics (Figs. 2d, 3a). When regional variability in the magnitude of slab overprinting is accounted for, it becomes clear that most arcs follow two-component mixing trends towards slab components that are clustered within $\delta^{11}B$ of 3‰ to 7‰. This may indicate similar overall dehydration systematics and across-arc melt transport mechanisms in these arcs. The SAVZ has a slab component with slightly lower $\delta^{11}B$ (≈0‰). The Cascades also appear to have a low-$\delta^{11}B$ slab component (112, 113), but this arc is not included here due to the lack of mafic to intermediate

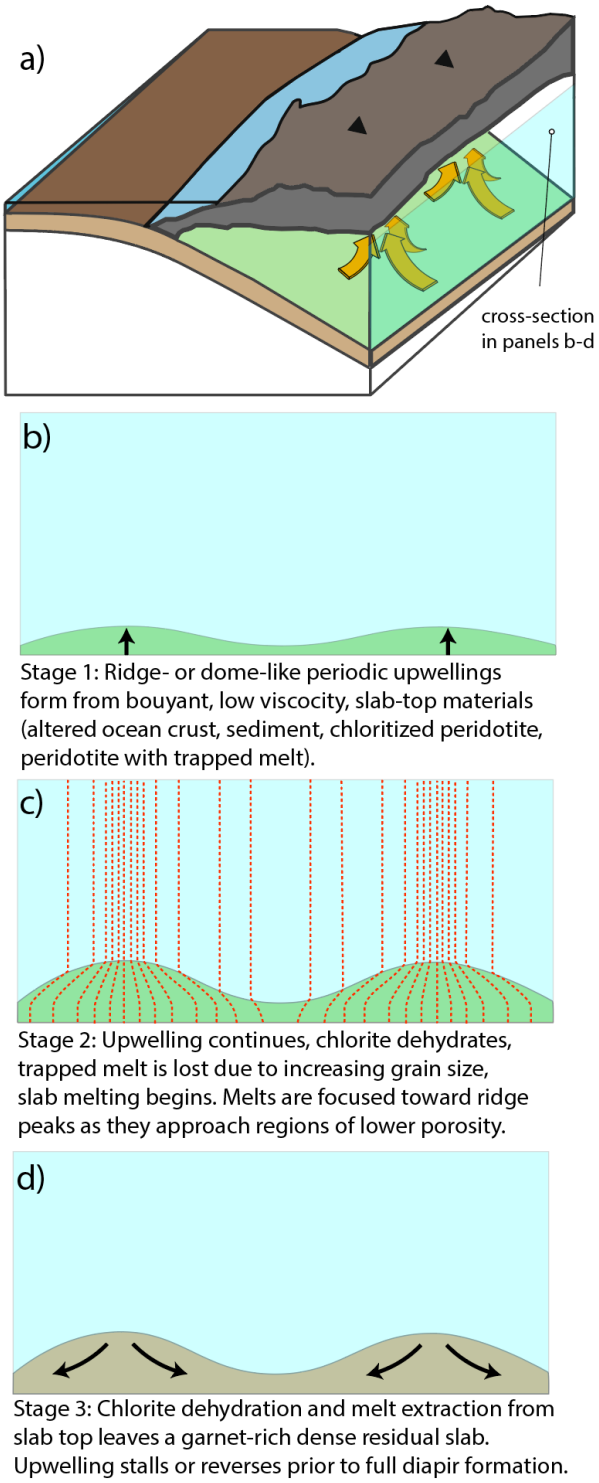

Figure 5. A conceptual model to account for along-strike variability in the distribution of slab liquids in the mantle wedge. See text for discussion.

samples from long-lived polygenetic arc-front stratovolcanoes with both $\delta^{11}B$ and comprehensive trace element data.

An explanation for the lower $\delta^{11}B$ of the SAVZ (and Cascades) slab component is that the shallow slab dip angle (red line in Fig 2c) and relatively young slab age cause more extensive dehydration and expulsion of high-$\delta^{11}B$ fluids beneath the forearc. The shallow subduction angle may also limit the distance over which deeper dehydration fluids can travel updip toward the arc front. The overall hotter slab thermal structure could also lead to less extensive serpentinization of the slab lithospheric mantle, less total isotopic fractionation between fluids and the residual slab, and an outsized role for slab melting. A quantitative test of these hypothesis requires a more sophisticated treatment of slab melting, which may significantly impact the stability of the B host-mineral phengite (19, 106, 114), but is beyond this paper's scope. Expanded studies of B isotopes in across-arc transects from other subduction zones with 'hot' slabs will help to further clarify the role of slab thermal structure in the future.

While the SAVZ provides a low- $\delta^{11}B$ global end member, the volcanics of South Sandwich are a notable high-$\delta^{11}B$ outlier (Fig. 2c), requiring an average slab component with $\delta^{11}B \approx 15‰$ (55). An earlier global analysis (39) indicated a possible relationship between $\delta^{11}B$ and the slab dip angle, which is especially steep beneath the South Sandwich Islands (Fig. 2d). New data from Nicaragua (18), however, which has similarly steep slab geometry (Fig. 2d), indicates a slab component with $\delta^{11}B \approx 4‰$, in line with most other arcs (Fig. 2c). The varied compositions of Nicaragua and South Sandwich thus appear to contradict the hypothesis that slab geometry is a dominant factor. A comparison between slab profiles and data from the SAVZ and Honshu are also inconsistent with control by slab geometry, given that Honshu has the shallowest slab profile on Fig. 2c and a dip angle similar to the SAVZ, but overlies the Marianas and Kamchatka in $\delta^{11}B$ vs Ce/B (Fig. 2a). It is likely that the compositional difference between Honshu and the SAVZ instead arises due to the fact that the slab beneath Honshu is older by ~100 My (2).

It is possible that the distinct $\delta^{11}B$ composition of South Sandwich, on the other hand, is related to the distinct texture of the subducting oceanic crust. The crust subducting beneath South Sandwich was generated in the slow spreading South American-Antarctic ridge and is remarkably fractured, whereas the crust subducting beneath Nicaragua is devoid of fracture zones (Fig. S2). Direct sampling of fractured ocean crust has revealed anomalously high $\delta^{11}B$ (76), and links between fracture zones and high-$\delta^{11}B$ volcanics have also been proposed for more felsic samples from the Lesser Antilles (115). The composition of the downgoing oceanic crust may have an outsized influence on the composition of the slab components expressed in each arc (18), and may thus account for the anomalous data from South Sandwich.

Finally, we note that if the compositional differences in the mantle beneath small cones vs major stratovolcanoes are confirmed in other subduction zones, this would have important implications for studies of global arc systematics, older volcanic samples, and volatile element data measured in melt inclusions. Many melt-inclusion studies of arc volatile fluxes have focused primarily on monogenetic cones because they are usually more primitive and erupt scoria that is rapidly quenched. The presence of local geochemical differences between minor cones and stratovolcanoes indicates that it may be misleading to compare monogenetic cone data from one arc with stratovolcano data from another – especially if the aim of the comparison is to assess variations in subduction recycling efficiencies among arcs. This same concern applies for studies of older volcanic samples in which the sample locations relative to the paleo arc-front or the nature of their source vents are not well constrained. The regional geochemical context

presented here can be used to provide more robust comparison of regional and global datasets for future studies.

Materials and Methods Summary

All measurements were conducted on glassy melt inclusions within olivine crystals. This approach mitigates the potential effects of crustal contamination and secondary alteration (36, 37). Melt-inclusion bearing olivines were picked from the 250-500 µm size fraction. The olivines were mounted in acrylic and their inclusions exposed by grinding. Exposed melt inclusions were then re-mounted in indium and polished for analysis. Melt inclusions and their host olivines were analyzed for major elements via electron microprobe at Washington University in St. Louis using analytical conditions as described in (18). Melt inclusions were analyzed for $\delta^{11}B$ via established techniques on the Cameca IMS-1270 at the NERC Edinburgh Ion Microprobe Facility (EIMF), as described in detail by (116). Instrumental fractionation was corrected using a linear standard calibration (R^2=99.5) consisting of StHs6/80-G ($\delta^{11}B$=-4.4‰), B6 ($\delta^{11}B$=-1.8‰), GSD1-G ($\delta^{11}B$=10.2‰), GOR128-G ($\delta^{11}B$=13.6‰), and BCR2-G ($\delta^{11}B$=-5.9‰). Abundances of B, Ce, Sr, H_2O, and CO_2 were measured in the glass inclusions using the EIMF Cameca IMS-4f, again following established techniques as described in (116) or via NanoSIMS and the IMS-6f at the Carnegie institute following the methods of (117). Measured compositions and analytical uncertainties are reported in Supplementary Table 1.

The implementation of the slab dehydration and boron-loss model shown in Figure 3 is as described in Turner et al., (2023), but with three major improvements. First, the H_2O capacity of the mafic ocean crust is based directly on the experimentally determined bounds from Schmidt and Poli (1998) or Forneris and Holloway (2003) rather than a thermodynamic/petrological model. Second, each time a fluid is generated, it now moves vertically up the slab, with the fluid and residual solid composition recalculated at each step assuming 100% re-equilibration. This implementation is carried out as described in Konrad-Schmolke et al. (2014, 2016). And third, phengite in the sediment layer is set to decrease linearly from the sediment solidus at 725 C until exhaustion at 850 C, in order to be consistent with the radiolarian clay melting experiments of Skora et al (2010).

For each interval of slab dehydration, the liquid H_2O/Ce is calculated using the parameterization of Cooper et al. (2012) [H_2O/Ce=exp(16.81-0.0109*(T-2.5*(-D-124)))], based on the average temperature (T) of the top 1 km of the slab at a given slab top depth (D, in km). Ce/B is then calculated using the liquid B concentrations output by the dehydration model, assuming liquids have 50% H_2O. The assumed H_2O concentration of the slab liquids have no impact of the model interpretation, though a lower assumed water content would shift the modeled Ce/B to slightly lower values on Figure 3d (and still fail to reproduce the linear mixing trends observed in the data). Because the Cooper et al. (2012) H_2O/Ce parameterization is only applicable when the slab surface exceeds the water saturated sediment solidus, a separate parameterization is used at colder temperatures (prior to the slab surface reaching 725 °C). In this case, the Ce concentration of slab fluids is calculated based on a $D^{solid/fluid}$ value for LREE of 700 (118), and the bulk sediment Ce concentration of 31.5 ppm (119).

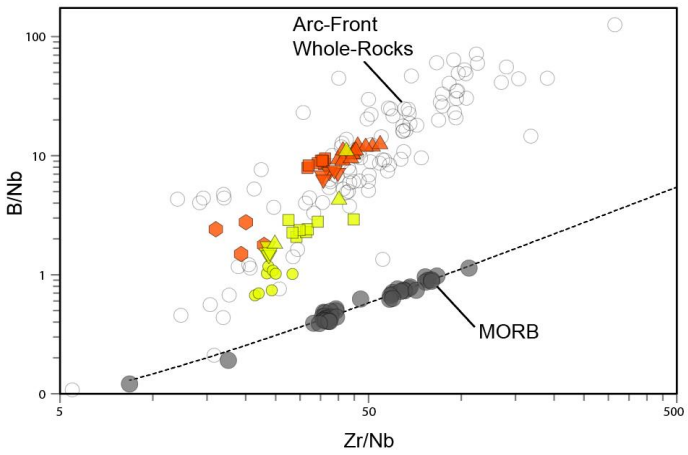

Figure S1. Data from MORB, our SAVZ samples, and other arcs (open circles)

The ratio Zr/Nb is also useful for understanding the composition of the 'ambient' mantle material feeding the arc mantle wedge because neither Zr nor Nb are transferred significantly from the slab (see Turner and Langmuir 2022a,b,c, and references within). The global correlation between Zr/Nb and B/Nb within the global arc-front data suggests that variations in arc B/Nb are controlled not only by the slab component, but also by the composition of the ambient mantle. Subduction zones near back-arc spreading centers have ambient mantle sources that are even more depleted than MORB (Woodhead et al., 1993). These very high Zr/Nb arcs thus have ambient mantle sources with even higher B/Nb than MORB. Arc ambient mantle B/Nb ratios are thus likely to vary globally by a factor of 15, and as such this ratio is inappropriate for typical interpretations of arc data, especially on a global scale.

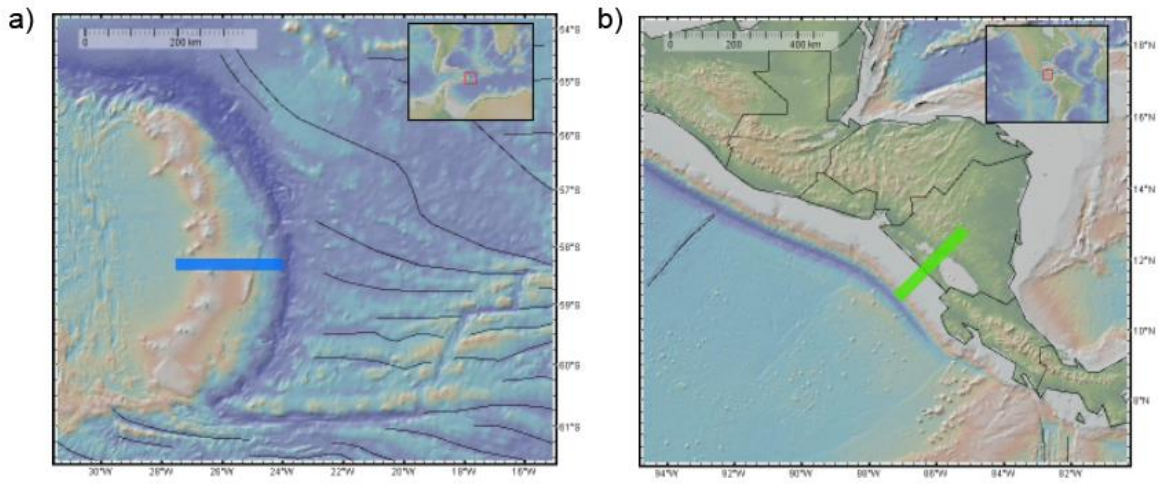

Figure S2. A comparison of the bathymetry offshore of a) South Sandwich Islands, and **b)** Nicaragua. Lines indicate the approximate transects shown on Fig 2c. The incoming seafloor in South Sandwich was generated in an ultra-slow spreading center and is incredibly fractured, which likely contributes to the composition of the related arc volcanics.

596

Citations

1. Implementation Plan | SZ4D. Available at: https://www.sz4d.org/implementation-plan [Accessed 10 June 2024].

2. E. M. Syracuse, P. E. van Keken, G. A. Abers, The global range of subduction zone thermal models. *Physics of the Earth and Planetary Interiors* **183**, 73–90 (2010).

3. L. B. Cooper, *et al.*, Global variations in H2O/Ce: 1. Slab surface temperatures beneath volcanic arcs. *Geochemistry, Geophysics, Geosystems* **13** (2012).

4. D. M. Ruscitto, P. J. Wallace, L. B. Cooper, T. Plank, Global variations in H2O/Ce: 2. Relationships to arc magma geochemistry and volatile fluxes. *Geochemistry, Geophysics, Geosystems* **13** (2012).

5. C. E. Manning, The chemistry of subduction-zone fluids. *Earth Planet Sci Lett* **223**, 1–16 (2004).

6. A. M. Cagnioncle, E. M. Parmentier, L. T. Elkins-Tanton, Effect of solid flow above a subducting slab on water distribution and melting at convergent plate boundaries. *J Geophys Res Solid Earth* **112**, 9402 (2007).

7. N. G. Cerpa, I. Wada, C. R. Wilson, Fluid migration in the mantle wedge: Influence of mineral grain size and mantle compaction. *J Geophys Res Solid Earth* **122**, 6247–6268 (2017).

8. M. Spiegelman, D. McKenzie, Simple 2-D models for melt extraction at mid-ocean ridges and island arcs. *Earth Planet Sci Lett* **83**, 137–152 (1987).

9. C. R. Wilson, M. Spiegelman, P. E. van Keken, B. R. Hacker, Fluid flow in subduction zones: The role of solid rheology and compaction pressure. *Earth Planet Sci Lett* **401**, 261–274 (2014).

10. J. Nakajima, *et al.*, Seismic attenuation beneath northeastern Japan: Constraints on mantle dynamics and arc magmatism. *J Geophys Res Solid Earth* **118**, 5838–5855 (2013).

11. I. Wada, J. He, A. Hasegawa, J. Nakajima, Mantle wedge flow pattern and thermal structure in Northeast Japan: Effects of oblique subduction and 3-D slab geometry. *Earth Planet Sci Lett* **426**, 76–88 (2015).

12. G. Zhu, T. V. Gerya, S. Honda, P. J. Tackley, D. A. Yuen, Influences of the buoyancy of partially molten rock on 3-D plume patterns and melt productivity above retreating slabs. *Physics of the Earth and Planetary Interiors* **185**, 112–121 (2011).

13. G. Zhu, *et al.*, Three-dimensional dynamics of hydrous thermal-chemical plumes in oceanic subduction zones. *Geochemistry, Geophysics, Geosystems* **10** (2009).

14. D. W. Rees Jones, H. Zhang, R. F. Katz, Magmatic channelization by reactive and shear-driven instabilities at mid-ocean ridges: a combined analysis. *Geophys J Int* **226**, 582–609 (2021).

15. T. Gerya, Numerical modeling of subduction: State of the art and future directions. *Geosphere* **18**, 503–561 (2022).

16. R. F. Katz, D. W. R. Jones, J. F. Rudge, T. Keller, Physics of Melt Extraction from the Mantle: Speed and Style. *https://doi.org/10.1146/annurev-earth-032320-083704* **50**, 507–540 (2022).

17. P. B. Kelemen, G. Hirth, N. Shimizu, M. Spiegelman, H. J. B. Dick, A review of melt migration processes in the adiabatically upwelling mantle beneath oceanic spreading ridges. *Philosophical Transactions of the Royal Society of London. Series A: Mathematical, Physical and Engineering Sciences* **355**, 283–318 (1997).

18. S. J. Turner, *et al.*, Boron isotopes in Central American volcanics indicate a key role for the subducting oceanic crust. *Earth Planet Sci Lett* **619**, 118289 (2023).

19. H. R. Marschall, R. Altherr, L. Rüpke, Squeezing out the slab — modelling the release of Li, Be and B during progressive high-pressure metamorphism. *Chem Geol* **239**, 323–335 (2007).

20. M. Konrad-Schmolke, R. Halama, Combined thermodynamic–geochemical modeling in metamorphic geology: Boron as tracer of fluid–rock interaction. *Lithos* **208–209**, 393–414 (2014).

21. M. Konrad-Schmolke, R. Halama, V. C. Manea, Slab mantle dehydrates beneath Kamchatka-yet recycles water into the deep mantle. *Geochemistry, Geophysics, Geosystems* **17**, 2987–3007 (2016).

22. N. G. Cerpa, I. Wada, C. R. Wilson, Effects of fluid influx, fluid viscosity, and fluid density on fluid migration in the mantle wedge and their implications for hydrous melting. *Geosphere* **15**, 1–23 (2019).

23. P. Bird, An updated digital model of plate boundaries. *Geochemistry, Geophysics, Geosystems* **4**, 1027 (2003).

24. G. Jacques, *et al.*, Geochemical variations in the Central Southern Volcanic Zone, Chile (38–43 S): The role of fluids in generating arc magmas. *Chem Geol* **371**, 27–45 (2014).

25. G. Jacques, *et al.*, Across-arc geochemical variations in the Southern Volcanic Zone, Chile (34.5–38.0 S): constraints on mantle wedge and slab input compositions. *Geochim Cosmochim Acta* **123**, 218–243 (2013).

26. P. E. Wieser, *et al.*, New constraints from Central Chile on the origins of enriched continental compositions in thick-crusted arc magmas. *Geochim Cosmochim Acta* **267**, 51–74 (2019).

27. Y. W. Chen, J. Wu, J. Suppe, Southward propagation of Nazca subduction along the Andes. *Nature 2019 565:7740* **565**, 441–447 (2019).

28. E. Contreras-Reyes, I. Grevemeyer, E. R. Flueh, C. Reichert, Upper lithospheric structure of the subduction zone offshore of southern Arauco peninsula, Chile, at ∼38°S. *J Geophys Res Solid Earth* **113**, 7303 (2008).

29. R. M. Conrey, D. R. Sherrod, P. R. Hooper, D. A. Swanson, Diverse primitive magmas in the Cascade arc, northern Oregon and southern Washington. *The Canadian Mineralogist* **35**, 367–396 (1997).

30. D. Sellés, M. Dungan, C. Langmuir, A. C. Rodríguez, W. P. Leeman, Magma and Mineral Composition Response to Increasing Slab-Derived Fluid Flux: Nevado de Longaví Volcano, Southern Chilean Andes. *Front Earth Sci (Lausanne)* **10**, 846997 (2022).

31. Sellés D, Rodriguez AC, Dungan MA, Naranjo JA, Gardeweg M, Geochemistry of Nevado de Longavi Volcano (36.2 degrees S): a compositionally atypical arc volcano in the Southern Volcanic Zone of the Andes. *Revista geológica de Chile* **31**, 293–315 (2004).

32. S. J. Turner, C. H. Langmuir, R. F. Katz, M. A. Dungan, S. Escrig, Parental arc magma compositions dominantly controlled by mantle-wedge thermal structure. *Nat Geosci* **9**, 772–776 (2016).

33. S. J. Turner, C. H. Langmuir, M. A. Dungan, S. Escrig, The importance of mantle wedge heterogeneity to subduction zone magmatism and the origin of EM1. *Earth Planet Sci Lett* **472**, 216–228 (2017).

34. D. R. Tormey, R. Hickey-Vargas, F. A. Frey, L. López-Escobar, Recent lavas from the Andean volcanic front (33 to 42 S); interpretations of along-arc compositional variations. *Geological Society of America Special Papers* **265**, 57–78 (1991).

35. N. Søager, P. M. Holm, E. J. Llambías, Payenia volcanic province, southern Mendoza, Argentina: OIB mantle upwelling in a backarc environment. *Chem Geol* **349**, 36–53 (2013).

36. W. P. Leeman, S. Tonarini, S. Turner, Boron isotope variations in Tonga-Kermadec-New Zealand arc lavas: Implications for the origin of subduction components and mantle influences. *Geochemistry, Geophysics, Geosystems* **18**, 1126–1162 (2017).

37. M. Rosner, J. Erzinger, G. Franz, R. B. Trumbull, Slab-derived boron isotope signatures in arc volcanic rocks from the Central Andes and evidence for boron isotope fractionation during progressive slab dehydration. *Geochemistry, Geophysics, Geosystems* **4** (2003).

38. H. R. Marschall, *et al.*, The boron and lithium isotopic composition of mid-ocean ridge basalts and the mantle. *Geochim Cosmochim Acta* **207**, 102–138 (2017).

39. J. C. M. De Hoog, I. P. Savov, Boron isotopes as a tracer of subduction zone processes. *Advances in Isotope Geochemistry* 217–247 (2018).

40. C. Spandler, C. Pirard, Element recycling from subducting slabs to arc crust: a review. *Lithos* **170**, 208–223 (2013).

41. B. Wunder, A. Meixner, R. Romer, R. Wirth, W. Heinrich, The geochemical cycle of boron: Constraints from boron isotope partitioning experiments between mica and fluid. *Lithos* **84**, 206–216 (2005).

42. K. J. Walowski, *et al.*, Boron recycling in the mantle: Evidence from a global comparison of ocean island basalts. *Geochim Cosmochim Acta* **302**, 83–100 (2021).

43. A. N. Paul, *et al.*, Refining Boron Isotopic Measurements of Silicate Samples by Multi-Collector-Inductively Coupled Plasma-Mass Spectrometry (MC-ICP-MS). *Geostand Geoanal Res* **48**, 91–108 (2024).

44. G. L. Foster, H. R. Marschall, M. R. Palmer, Boron Isotope Analysis of Geological Materials. *Advances in Isotope Geochemistry* 13–31 (2018). https://doi.org/10.1007/978-3-319-64666-4_2.

45. T. Ishikawa, E. Nakamura, Boron isotope geochemistry of the oceanic crust from DSDP/ODP Hole 504B. *Geochim Cosmochim Acta* **56**, 1633–1639 (1992).

46. H. J. Smith, A. J. Spivack, H. Staudigel, S. R. Hart, The boron isotopic composition of altered oceanic crust. *Chem Geol* **126**, 119–135 (1995).

47. T. Ishikawa, F. Tera, Source, composition and distribution of the fluid in the Kurile mantle wedge: Constraints from across-arc variations of B/Nb and B isotopes. *Earth Planet Sci Lett* **152**, 123–138 (1997).

48. T. Ishikawa, F. Tera, T. Nakazawa, Boron isotope and trace element systematics of the three volcanic zones in the Kamchatka arc. *Geochim Cosmochim Acta* **65**, 4523–4537 (2001).

49. J. G. Ryan, J. Morris, F. Tera, W. P. Leeman, A. Tsvetkov, Cross-Arc Geochemical Variations in the Kurile Arc as a Function of Slab Depth. *Science (1979)* **270**, 625–627 (1995).

50. W. P. Leeman, V. B. Sisson, Geochemistry of boron and its implications for crustal and mantle processes. *Reviews in Mineralogy* **33**, 645–708 (1996).

51. A. A. Iveson, *et al.*, Deciphering variable mantle sources and hydrous inputs to arc magmas in Kamchatka. *Earth Planet Sci Lett* **562**, 116848 (2021).

52. S. Tonarini, S. Agostini, C. Doglioni, F. Innocenti, P. Manetti, Evidence for serpentinite fluid in convergent margin systems: The example of El Salvador (Central America) arc lavas. *Geochemistry, Geophysics, Geosystems* **8** (2007).

53. T. Moriguti, T. Shibata, E. Nakamura, Lithium, boron and lead isotope and trace element systematics of Quaternary basaltic volcanic rocks in northeastern Japan: mineralogical controls on slab-derived fluid composition. *Chem Geol* **212**, 81–100 (2004).

54. T. Ishikawa, F. Tera, Two isotopically distinct fluid components involved in the Mariana arc: Evidence from Nb/B ratios and B, Sr, Nd, and Pb isotope systematics. *Geology* (1999). [Accessed 12 September 2023].

55. S. Tonarini, W. P. Leeman, P. T. Leat, Subduction erosion of forearc mantle wedge implicated in the genesis of the South Sandwich Island (SSI) arc: Evidence from boron isotope systematics. *Earth Planet Sci Lett* **301**, 275–284 (2011).

56. I. Grevemeyer, *et al.*, Heat flow and bending-related faulting at subduction trenches: Case studies offshore of Nicaragua and Central Chile. *Earth Planet Sci Lett* **236**, 238–248 (2005).

57. C. R. Ranero, J. Phipps Morgan, K. McIntosh, C. Reichert, Bending-related faulting and mantle serpentinization at the Middle America trench. *Nature* **425**, 367–373 (2003).

58. P. E. van Keken, I. Wada, G. A. Abers, B. R. Hacker, K. Wang, Mafic high-pressure rocks are preferentially exhumed from warm subduction settings. *Geochemistry, Geophysics, Geosystems* **19**, 2934–2961 (2018).

59. P. E. van Keken, B. R. Hacker, E. M. Syracuse, G. A. Abers, Subduction factory: 4. Depth-dependent flux of H 2 O from subducting slabs worldwide. *J Geophys Res* **116**, B01401 (2011).

60. B. R. Jicha, O. Jagoutz, Magma production rates for intraoceanic arcs. *Elements* **11**, 105–111 (2015).

741 61. L. D. Benton, J. G. Ryan, F. Tera, Boron isotope systematics of slab fluids as inferred from a
742 serpentine seamount, Mariana forearc. *Earth Planet Sci Lett* **187**, 273–282 (2001).

743 62. I. P. Savov, J. G. Ryan, M. D'Antonio, P. Fryer, Shallow slab fluid release across and along the
744 Mariana arc-basin system: Insights from geochemistry of serpentinized peridotites from the
745 Mariana fore arc. *J Geophys Res* **112**, B09205 (2007).

746 63. I. P. Savov, J. G. Ryan, M. D'Antonio, K. Kelley, P. Mattie, Geochemistry of serpentinized
747 peridotites from the Mariana Forearc Conical Seamount, ODP Leg 125: Implications for the
748 elemental recycling at subduction zones. *Geochemistry, Geophysics, Geosystems* **6** (2005).

749 64. J. B. Gill, Geophysical Setting of Volcanism at Convergent Plate Boundaries. 44–63 (1981).
750 https://doi.org/10.1007/978-3-642-68012-0_3.

751 65. I. Wada, K. Wang, Common depth of slab-mantle decoupling: Reconciling diversity and uniformity
752 of subduction zones: COMMON DEPTH OF SLAB-MANTLE DECOUPLING. *Geochemistry,*
753 *Geophysics, Geosystems* **10**, n/a–n/a (2009).

754 66. G. A. Abers, P. E. Van Keken, B. R. Hacker, The cold and relatively dry nature of mantle forearcs in
755 subduction zones. *Nature Geoscience 2017 10:5* **10**, 333–337 (2017).

756 67. P. C. England, R. F. Katz, Melting above the anhydrous solidus controls the location of volcanic
757 arcs. *Nature* **467**, 700–703 (2010).

758 68. T. L. Grove, C. B. Till, M. J. Krawczynski, The role of H2O in subduction zone magmatism. *Annu*
759 *Rev Earth Planet Sci* **40**, 413–439 (2012).

760 69. I. Wada, M. D. Behn, Focusing of upward fluid migration beneath volcanic arcs: Effect of mineral
761 grain size variation in the mantle wedge. *Geochemistry, Geophysics, Geosystems* **16**, 3905–3923
762 (2015).

763 70. D. M. Miller, S. L. Goldstein, C. H. Langmuir, Cerium/lead and lead isotope ratios in arc magmas
764 and the enrichment of lead in the continents. *Nature* **368**, 514–520 (1994).

765 71. T. Elliott, T. Plank, A. Zindler, W. White, B. Bourdon, Element transport from slab to volcanic front
766 at the Mariana arc. *Journal of Geophysical Research: Solid Earth (1978–2012)* **102**, 14991–15019
767 (1997).

768 72. C. Class, D. M. Miller, S. L. Goldstein, C. H. Langmuir, Distinguishing melt and fluid subduction
769 components in Umnak Volcanics, Aleutian Arc. *Geochemistry, Geophysics, Geosystems* **1** (2000).

770 73. S. J. Turner, C. H. Langmuir, An alternative to the igneous crust fluid + sediment melt paradigm
771 for arc lava geochemistry. *Science Advances (in press)* (2024).

772 74. S. S. Wei, *et al.*, Along-strike variations in intermediate-depth seismicity and arc magmatism
773 along the Alaska Peninsula. *Earth Planet Sci Lett* **563**, 116878 (2021).

774 75. A. Hammerstrom, R. Carlson, R. Parai, S. Turner, Seamounts control subducted carbonate
775 recycling in Central America – evidence from stable Sr isotopes. *Nature Communications (in*
776 *review)* (2024).

76. A. M. McCaig, *et al.*, No significant boron in the hydrated mantle of most subducting slabs. *Nat Commun* **9**, 4602 (2018).

77. R. Hickey-Vargas, *et al.*, Multiple subduction components in the mantle wedge: evidence from eruptive centers in the Central Southern volcanic zone, Chile. *Geology* **30**, 199–202 (2002).

78. R. Hickey-Vargas, S. Holbik, D. Tormey, F. A. Frey, H. M. Roa, Basaltic rocks from the Andean Southern Volcanic Zone: Insights from the comparison of along-strike and small-scale geochemical variations and their sources. *Lithos* **258**, 115–132 (2016).

79. H. Rawson, *et al.*, Compositional variability in mafic arc magmas over short spatial and temporal scales: Evidence for the signature of mantle reactive melt channels. *Earth Planet Sci Lett* **456**, 66–77 (2016).

80. V. J. M. Salters, A. Stracke, Composition of the depleted mantle. *Geochemistry, Geophysics, Geosystems* **5** (2004).

81. J. A. Pearce, D. W. Peate, Tectonic implications of the composition of volcanic arc magmas. *Annu Rev Earth Planet Sci* **23**, 251–286 (1995).

82. S. J. Turner, C. H. Langmuir, An Evaluation of Five Models of Arc Volcanism. *Journal of Petrology* **63** (2022).

83. S. J. Turner, C. H. Langmuir, A quantitative framework for global variations in arc geochemistry. *Earth Planet Sci Lett* **584**, 117411 (2022).

84. S. J. Turner, C. H. Langmuir, Sediment and ocean crust both melt at subduction zones. *Earth Planet Sci Lett* **584**, 117424 (2022).

85. A. Gómez-Tuena, L. Mori, S. M. Straub, Geochemical and petrological insights into the tectonic origin of the Transmexican Volcanic Belt. *Earth Sci Rev* **183**, 153–181 (2018).

86. E. Aharonov, J. A. Whitehead, P. B. Kelemen, M. Spiegelman, Channeling instability of upwelling melt in the mantle. *J Geophys Res Solid Earth* **100**, 20433–20450 (1995).

87. M. Spiegelman, P. B. Kelemen, E. Aharonov, Causes and consequences of flow organization during melt transport: The reaction infiltration instability in compactible media. *J Geophys Res Solid Earth* **106**, 2061–2077 (2001).

88. P. B. Kelemen, *et al.*, Spatial distribution of melt conduits in the mantle beneath oceanic spreading ridges: Observations from the Ingalls and Oman ophiolites. *Geochemistry, Geophysics, Geosystems* **1**, 1005 (2000).

89. P. B. Kelemen, H. J. B. Dick, J. E. Quick, Formation of harzburgite by pervasive melt/rock reaction in the upper mantle. *Nature 1992 358:6388* **358**, 635–641 (1992).

90. D. W. Rees Jones, R. F. Katz, Reaction-infiltration instability in a compacting porous medium. *J Fluid Mech* **852**, 5–36 (2018).

91. F. Selig, A theoretical prediction of salt dome patterns. *Geophysics* **30**, 633–643 (1965).

92. J. A. Whitehead, D. S. Luther, Dynamics of laboratory diapir and plume models. *J Geophys Res* **80**, 705–717 (1975).

93. B. D. Marsh, I. S. E. Carmichael, Benioff zone magmatism. *J Geophys Res* **79**, 1196–1206 (1974).

94. M. D. Behn, P. B. Kelemen, G. Hirth, B. R. Hacker, H.-J. Massonne, Diapirs as the source of the sediment signature in arc lavas. *Nat Geosci* **4**, 641–646 (2011).

95. D. Ghosh, G. Maiti, N. Mandal, A. Baruah, Cold Plumes Initiated by Rayleigh-Taylor Instabilities in Subduction Zones, and Their Characteristic Volcanic Distributions: The Role of Slab Dip. *J Geophys Res Solid Earth* **125**, e2020JB019814 (2020).

96. P. S. Hall, C. Kincaid, Diapiric flow at subduction zones: A recipe for rapid transport. *Science (1979)* **292**, 2472–2475 (2001).

97. T. V Gerya, D. A. Yuen, Rayleigh–Taylor instabilities from hydration and melting propel 'cold plumes' at subduction zones. *Earth Planet Sci Lett* **212**, 47–62 (2003).

98. M. C. Johnson, T. Plank, Dehydration and melting experiments constrain the fate of subducted sediments. *Geochemistry, Geophysics, Geosystems* **1** (2000).

99. T. Elliott, Tracers of the slab. *Geophysical Monograph-American Geophysical Union* **138**, 23–46 (2003).

100. C. Pirard, J. Hermann, Focused fluid transfer through the mantle above subduction zones. *Geology* **43**, 915–918 (2015).

101. H. Li, J. Hermann, L. Zhang, Melting of subducted slab dictates trace element recycling in global arcs. *Sci Adv* **8**, 2166 (2022).

102. P. B. Kelemen, K. Hanghøj, A. R. Greene, One view of the geochemistry of subduction-related magmatic arcs, with an emphasis on primitive andesite and lower crust. *Treatise on geochemistry* **3**, 659 (2003).

103. H. Freymuth, B. Ivko, J. B. Gill, Y. Tamura, T. Elliott, Thorium isotope evidence for melting of the mafic oceanic crust beneath the Izu arc. *Geochim Cosmochim Acta* **186**, 49–70 (2016).

104. G. M. Yogodzinski, *et al.*, Sr and O isotopes in western Aleutian seafloor lavas: Implications for the source of fluids and trace element character of arc volcanic rocks. *Earth Planet Sci Lett* **475**, 169–180 (2017).

105. S. Skora, J. Blundy, High-pressure Hydrous Phase Relations of Radiolarian Clay and Implications for the Involvement of Subducted Sediment in Arc Magmatism. *Journal of Petrology* **51**, 2211–2243 (2010).

106. U. Mann, M. W. Schmidt, Melting of pelitic sediments at subarc depths: 1. Flux vs. fluid-absent melting and a parameterization of melt productivity. *Chem Geol* **404**, 150–167 (2015).

107. D. W. Sparks, E. M. Parmentier, Melt extraction from the mantle beneath spreading centers. *Earth Planet Sci Lett* **105**, 368–377 (1991).

847 108. M. Spiegelman, Physics of melt extraction: theory, implications and applications. *Philosophical*
848 *Transactions of the Royal Society of London. Series A: Physical and Engineering Sciences* **342**, 23–
849 41 (1993).

850 109. T. Keller, R. F. Katz, M. M. Hirschmann, Volatiles beneath mid-ocean ridges: Deep melting,
851 channelised transport, focusing, and metasomatism. *Earth Planet Sci Lett* **464**, 55–68 (2017).

852 110. A. J. Turner, R. F. Katz, M. D. Behn, T. Keller, Magmatic Focusing to Mid-Ocean Ridges: The Role of
853 Grain-Size Variability and Non-Newtonian Viscosity. *Geochemistry, Geophysics, Geosystems* **18**,
854 4342–4355 (2017).

855 111. S. J. Sim, M. Spiegelman, D. R. Stegman, C. Wilson, The influence of spreading rate and
856 permeability on melt focusing beneath mid-ocean ridges. *Physics of the Earth and Planetary*
857 *Interiors* **304**, 106486 (2020).

858 112. W. P. Leeman, S. Tonarini, L. H. Chan, L. E. Borg, Boron and lithium isotopic variations in a hot
859 subduction zone—the southern Washington Cascades. *Chem Geol* **212**, 101–124 (2004).

860 113. K. J. Walowski, P. J. Wallace, M. A. Clynne, D. J. Rasmussen, D. Weis, Slab melting and magma
861 formation beneath the southern Cascade arc. *Earth Planet Sci Lett* **446**, 100–112 (2016).

862 114. M. W. Schmidt, D. Vielzeuf, E. Auzanneau, Melting and dissolution of subducting crust at high
863 pressures: the key role of white mica. *Earth Planet Sci Lett* **228**, 65–84 (2004).

864 115. G. F. Cooper, *et al.*, Variable water input controls evolution of the Lesser Antilles volcanic arc.
865 *Nature 2020 582:7813* **582**, 525–529 (2020).

866 116. K. J. Walowski, *et al.*, Investigating ocean island mantle source heterogeneity with boron isotopes
867 in melt inclusions. *Earth Planet Sci Lett* **508**, 97–108 (2019).

868 117. E. H. Hauri, *et al.*, CO2 content beneath northern Iceland and the variability of mantle carbon.
869 *Geology* **46**, 55–58 (2018).

870 118. C. Spandler, J. Mavrogenes, J. Hermann, Experimental constraints on element mobility from
871 subducted sediments using high-P synthetic fluid/melt inclusions. *Chem Geol* **239**, 228–249
872 (2007).

873 119. T. Plank, The chemical composition of subducting sediments. *The Crust, Treatise on Geochemistry*
874 **4** (2013).

875